www.MaterialsViews.com

ADVANCED
ENERGY
MATERIALS
www.advenergymat.de

COMMUNICATION

Elastomeric and Dynamic MnO₂/CNT Core–Shell Structure Coiled Yarn Supercapacitor

Changsoon Choi, Hyeon Jun Sim, Geoffrey M. Spinks, Xavier Lepró, Ray H. Baughman, and Seon Jeong Kim*

1D yarn/fiber supercapacitors are more attractive power sources than conventional 3D, 2D foam/film-type when they are used for miniaturized electronic devices, textile electronics, and implantable medical devices[1] because their small volume and high flexibility enable them to be easily integrated into the devices with a tiny size and various shapes. Nevertheless, most fiber-based supercapacitors (FBSs) simply possess the flexibility with limited tensile strain and stretchability[2–16] because they are mostly based on nonstretchable electrodes such as carbon nanotube (CNT) spun yarn,[2–7] graphene fiber,[8–12] carbon fiber,[13,14] and metal wire.[15] This lack of stretchability of these FBSs leads to limitation for more advanced utilization, e.g., as a power source for artificial muscles[17] or wearable devices that are exposed to high strain, especially in the joint part.[18] In recent years, several strategies have been reported to incorporate stretchability into FBSs: CNT sheet nanomembranes were wound onto elastic fibers to make highly stretchable FBSs[19–21] or CNT fiber electrodes were attached onto prestrained elastic fibers to form a microbuckling structure for FBSs.[22,23] Although these FBSs exhibited stable stretchability and energy storage performances, they still suffer from low electrochemical energy storage performance because the additional core fibers used as elastomeric substrates do not participate in electrochemical energy storage reactions but merely provide stretchability, resulting in low gravimetric and volumetric energy storage performances of the total devices.[24] To solve these problems, novel spring-like stretchable CNT fibers were proposed as supercapacitor electrodes.[24] It is notable that stretchability could be achieved for the first time in FBSs by using the spring CNT fiber without the help of any elastomeric substrate. However, the spring-based supercapacitors still showed limited capacitances because their active material was based on pristine CNT, totally depending on the electrochemical double layer capacitance (EDLC) energy storage mechanism. All things considered, achieving FBSs possessing not only stretchability but also excellent specific capacitances remains challenging.

In this study, we present coil-structured, pseudocapacitive yarns as promising electrodes for achieving stretchable and highly performing supercapacitors. The bare CNT coiled yarns are fabricated by inserting a giant twist (50 000 twists m^{-1}) into CNT spun yarns, which are drawn from a multiwalled carbon nanotube (MWNT) forest.[25] Although the bare CNT coiled yarns can be used as stretchable electrodes for EDLC-based supercapacitor without further processing,[24] we deposited MnO₂, which is a promising pseudocapacitive material because of its high theoretical capacitance, low cost, and environmental friendliness[26] to enhance dramatically its energy storage capacity. A scanning electron microscope (SEM) image of our novel core(CNT)–shell(MnO₂)-structured hybrid coiled yarn is shown in **Figure 1**A. The diameter of the single hybrid coiled electrode is ≈80 μm and about 200 uniform microloops are contained in a centimeter of coiled electrode. The resulting aspect ratio (ratio of coiled electrode's length to diameter) is high (about 210) and the electrode volume is impressively small (≈6.5 × 10^{-5} cm^3) that the volume of presented coiled CNT electrode is one-twentieth the size of previously reported coiled CNT/nylon fiber.[21]
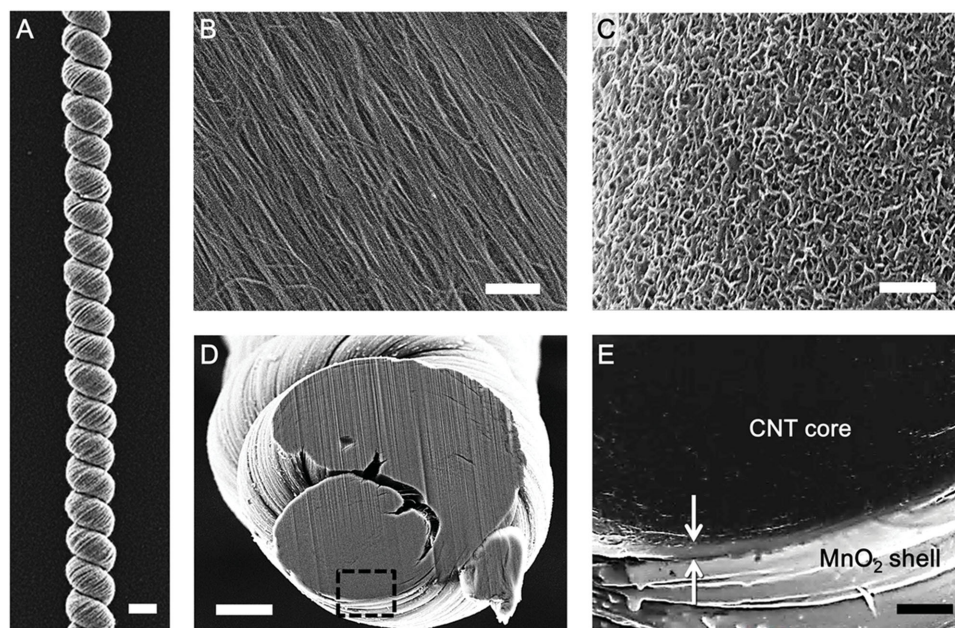
A high-resolution SEM surface image of the bare CNT coiled yarn (Figure 1B) shows closely packed and uniaxially aligned CNT bundles, which implies an effective electron pathway for longitudinal current collecting. After the MnO₂ deposition (Figure 1C), a mesoporous film, which is morphologically characteristic of MnO₂,[27] is uniformly formed on the surface of the coiled electrode. It is experimentally confirmed that strong adhesion of the MnO₂ thin shell to the porous CNT surface is achieved so that high electrochemical stability could be demonstrated against repeated mechanical deformation by loop opening or electrochemical reaction, which will be discussed later. In this study, the mass of MnO₂ was measured using an electrochemical quartz-crystal microbalance (EQCM). From the slope of the charge–mass graph measured by EQCM, the mass of MnO₂ per unit charge transferred during deposition is determined to be 5.4 × 10^{-4} g C^{-1}, as shown in Figure S1 in the Supporting Information. To measure the thickness of the MnO₂ shell layer, cross-sectional analysis was performed by cutting the hybrid coiled electrode along its diameter using a Ga ion beam, as shown in Figure 1D. Figure 1E shows a magnified SEM image of the denoted rectangle at the edge part of the hybrid coiled yarn cross-section shown in Figure 1D. The nanoscopic MnO₂ shell with thickness ≈1 μm is distinguished from the CNT core part. Because only nanoscopic surfaces of MnO₂

C. Choi, H. J. Sim, Prof. S. J. Kim
Center for Self-Powered Artificial Muscle
and Department of Biomedical Engineering
Hanyang University
Seoul 04763, Korea
E-mail: sjk@hanyang.ac.kr
Prof. G. M. Spinks
Intelligent Polymer Research Institute
ARC Centre of Excellence for Electromaterials Science
University of Wollongong
Wollongong, NSW 2522, Australia
Dr. X. Lepró, Prof. R. H. Baughman
The Alan G. MacDiarmid Nano Tech Institute
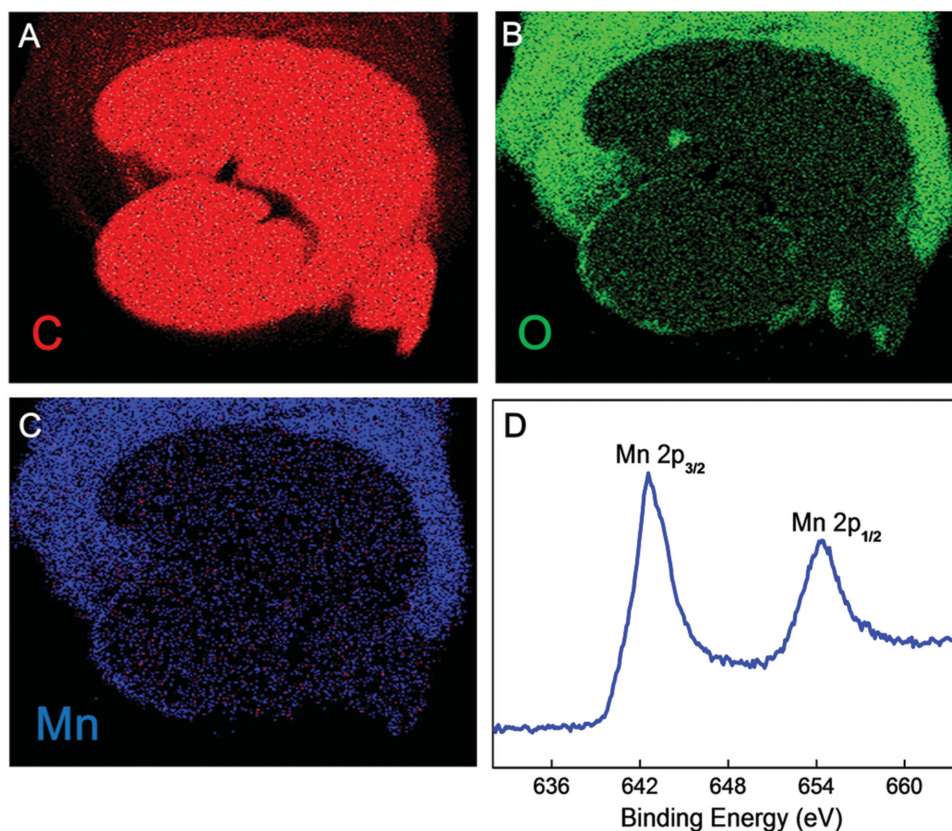University of Texas at Dallas
Richardson, TX 75083, USA

ADVANCED
ENERGY
MATERIALS
www.advenergymat.de

Materials
Views
www.MaterialsViews.com

COMMUNICATION

Figure 1. Overview SEM image of A) MnO_2/CNT core–shell-structured coiled electrode (scale bar = 50 μm). Its magnified surface images of B) before (scale bar = 1 μm) and C) after MnO_2 deposition onto the bare coiled yarn (scale bar = 400 nm). Uniaxially aligned bare CNT electrode's surface is covered by mesoporous and nanoscopic MnO_2 film after deposition, constructing a core(CNT)–shell(MnO_2)-structured yarn electrode. Cross-sectional SEM images of D) MnO_2/CNT coiled yarn electrode (scale bar = 20 μm) and E) magnification of the edge part indicated by a square in (D) (scale bar = 3 μm). The MnO_2 shell is denoted by arrows. Volume and weight ratio of MnO_2 shell to total coiled electrode are calculated to be 4.9% and 17.2%, respectively.

can participate in the electrochemical energy storage reaction, the loading amount of MnO_2 is controlled by adjusting its deposition time to have a thin shell with reasonable thickness (≈1 μm) to obtain high capacitances and high-rate capability, simultaneously. As a consequence, volume and weight fractions of presented MnO_2 shell to total hybrid coiled electrode are calculated to be 4.9% and 17.2%, respectively. This pseudocapacitive microshell plays a crucial role in enhancing energy storage performances of yarn supercapacitors.

Energy dispersive spectroscopy (EDS) analysis was performed to characterize clearly the hybrid core–shell structure of the electrode. Elemental mapping analysis for C, O, and Mn atoms was performed on the Figure 1D image to detect the location of specific atoms, as shown in **Figure 2**A–C. The core part of the hybrid coiled electrode has highly densified CNT without any observable pores. This pure CNT core is well distinguished by dominant C atoms' detection (denoted by red dots, Figure 2A) while the shell part is mainly detected by O atoms (green dots, Figure 2B) and Mn atoms (blue dots, Figure 2C). Clearer identification of atomic core–shell structure can be confirmed through the overlapped C, O, Mn mapping images (Figure S2, Supporting Information). Figure 2D indicates X-ray photoelectron spectroscopy (XPS) analysis of the deposited MnO_2 film. The binding energy difference between Mn $2p_{3/2}$ and Mn $2p_{1/2}$ peaks is about 11.8 eV, which exactly matches the value for MnO_2.[28] Therefore, it can be concluded that this nonvacuum-based, scalable, and cost-effective electrochemical deposition technique achieves successful core–shell structure formation for stretchable, pseudocapacitive yarn electrodes.

Figure 3A schematically illustrates the configuration of a complete solid-state, stretchable, and highly performing coiled

supercapacitor. Two symmetric pseudocapacitive coiled electrodes were assembled in a parallel direction with constant gap and coated with aqueous poly(vinyl alcohol) (PVA)-based gel containing lithium chloride (LiCl) with thickness around 20 μm. Figure 3B shows cyclic voltammogram (CV) curves of bare coiled CNT and MnO_2/CNT core–shell-coiled electrodes. Although the MnO_2 content is relatively small compared with the total electrode (4.9% volume fraction or 17.2% weight fraction), it achieves about 512% capacitance enhancement by the pseudocapacitive effect. Figure 3C shows CV curves of the solid-state coiled yarn supercapacitor measured with scan rates from 10 to 100 mV s^{-1}. The box-like rectangular-shaped CV curves without any redox peak well represent the pseudocapacitive characteristics of our coiled supercapacitor. The rectangular-shaped CV curves could be retained for high scan rates up to 500 mV s^{-1} (Figure S3, Supporting Information), showing high-rate capability. Figure 3D shows the Nyquist curve of the coiled supercapacitor. A vertical curve indicates an excellent capacitive characteristic of the coiled supercapacitor. Moreover, low equivalent series resistance (ESR) as small as 0.07 Ω cm^3 is achieved (inset of Figure 3D). To inspect the charge/discharge characteristic of the coiled supercapacitor, galvanostatic curves at current densities of 0.2, 0.6, and 2 A cm^{-3} were measured (Figure S4, Supporting Information). Symmetrical triangle-shaped galvanostatic curves show good agreement with Nyquist analysis, indicating the excellent pseudocapacitive characteristics of the coiled supercapacitor. The specific capacitances based on single electrode were calculated from the CV curves as shown in Figure 3E. High volumetric capacitance (C_V, 34.6 F cm^{-3}), areal capacitance (C_A, 61.25 mF cm^{-2}), and linear capacitance (C_L, 2.72 mF cm^{-1}) could be achieved at 10 mV s^{-1} scan rate. The

www.MaterialsViews.com

**ADVANCED
ENERGY
MATERIALS**
www.advenergymat.de

COMMUNICATION

Figure 2. Elemental mapping analysis performed on the coil cross-section area and the location of A) C (carbon, red dots), B) O (oxygen, green dots), and C) Mn (manganese, blue dots) atoms are spotted. D) XPS analysis on MnO_2 shell. The binding energy difference between the Mn 2p doublet peaks is 11.8 eV, which corresponds to that expected for MnO_2.[21]

gravimetric capacitance (C_M) can be calculated about 26.5 F g^{-1} for the coiled supercapacitor. Dimensions of the total electrodes (both MnO_2/CNT coiled yarns) were used for normalization of specific capacitance. Moreover, high volumetric and areal energy densities (2.4 mWh cm^{-3} and 8.5 µWh cm^{-2}) were achieved in our stretchable fiber supercapacitor. The maximum capacitance values at 10 mV s^{-1} are retained to about 71.6% at 100 mV s^{-1} and 39% at 500 mV s^{-1}, showing high-rate capability (Figure S3, Supporting Information).

Specific capacitances of the coiled supercapacitors are compared with other FBSs in **Table 1**. Notably, the coiled supercapacitor exhibited much higher linear and areal capacitances (2.72 mF cm^{-1}, 61.25 mF cm^{-2}) than reported stretchable FBSs based on buckled CNT fiber (0.26 mF cm^{-1}, 27.98 mF cm^{-2})[23] and CNT spring fiber (0.51 mF cm^{-1}, 27.07 mF cm^{-2})[24] as shown in Table 1. It should be noted that the volumetric capacitance of the presented coiled supercapacitor (34.6 F cm^{-3}) was also excellent that about 10 times higher than our previous research on nylon fiber based stretchable supercapacitor (3.8 F cm^{-3})[21] without sacrificing linear and areal capacitances. These high specific capacitances were originated from effectively minimized volume of pristine CNT-based coiled fibers (only 5.2% volume of previous stretchable fiber)[21] by not using any elastomeric substrates. Moreover, the observed specific capacitances are remarkably higher than other reported hybrid FBSs, which do not offer the benefits of reversible elastomeric

deformability. For example, the volumetric capacitance of our coiled supercapacitor (34.6 F cm^{-3}) is about 14 times higher than MnO_2/carbon FBS (2.5 F cm^{-3})[13] and 7 times higher than MoS_2-reduced graphene oxide/CNT FBS (4.8 F cm^{-3})[7]. Moreover, its linear capacitance (2.72 mF cm^{-1}) is two orders higher than MnO_2/CNT FBS (0.019 mF cm^{-1}),[2] MnO_2/ZnO nanowire-coated FBS (0.02 mF cm^{-1}),[13] and also significantly higher than CNT/reduced graphene oxide fiber (0.35 mF cm^{-1}).[11] Such high specific capacitances of our coiled supercapacitor compared with other FBSs can be attributed to the following two aspects. The first is that nanoscopic, mesoporous, and pseudocapacitive metal oxide coating effectively enables high energy storage performance, without sacrificing the high-rate capability or mechanical stretchability. Second, neither additional elastomeric substrate nor separator is used in our coiled supercapacitor system, dramatically minimizing the total dimension of the electrodes.

Figure 4A shows optical images of the complete coiled supercapacitor before and after 37.5% strain was applied. Although the theoretical maximum strain is much higher for coiled CNT yarn (about more than 300% strain, which originates from the relation L(coiled yarn length) $\approx l$(initial yarn length)$/\pi$),[29] we present 37.5% as the maximum strain for a coiled supercapacitor. Because the applied strain rate for static tests in this study is much faster (180 mm min^{-1} or 2% s^{-1}) than the literature[29] (0.5 mm min^{-1} strain rate, 15 min intermediate stress relaxation
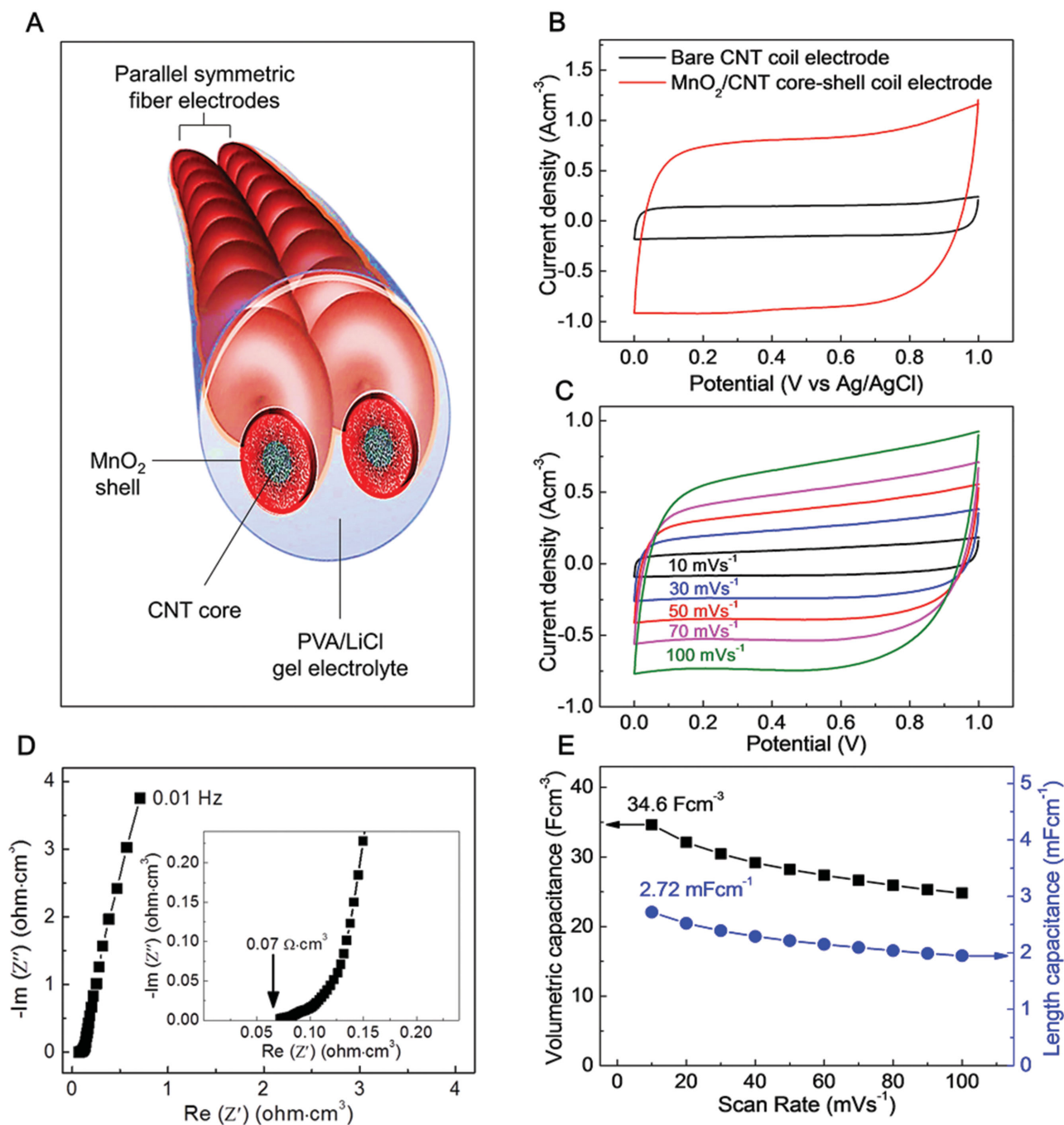
Figure 3. A) Schematic illustration for the complete solid-state coiled supercapacitor, which comprises two symmetric MnO_2/CNT core-–shell-coiled electrodes and gel electrolyte. B) CV curve comparison before and after MnO_2 deposition onto the bare coiled yarn. As a consequence of the pseudocapacitive contribution of the nanoscopic MnO_2 shell, the CV area increased by about 512% after MnO_2 deposition. C) CV curves of solid-state coiled supercapacitor measured from 10 to 100 mV s^{-1} scan rates. D) Nyquist curve shows a low ESR value of 0.07 Ω cm^{-3} around a high frequency of 100 kHz (inset) and vertical line. E) Calculated volumetric and linear capacitances of solid-state coiled supercapacitor for various scan rates. The highest volumetric and linear capacitances (based on the dimensions of both MnO_2/CNT coiled electrodes) are 34.6 F cm^{-3} and 2.72 mF cm^{-1} at 10 mV s^{-1} scan rate, respectively.

every strain increment) that not enough relaxation time is provided to uniformly relax the generated internal stresses during stretching and this results in early fracture for the coiled yarn (≈40% in tensile strain). In spite of such an early fracture, we adopted high strain rates (2%–6% s^{-1} or 180–540 mm min^{-1}

for dynamic tests) based stretching tests to reflect the real circumstances of wearable applications. The size of the tested supercapacitor was so small that it looks like a thin single thread to the naked eye, as shown in Figure 4A. Mechanical strain loading/unloading cycles were performed by applying

Table 1. Specific capacitance comparison of the coiled supercapacitor with reported FBSs.

Deformability	Electrode materials[REF]	C_L [mF cm^{-1}]	C_A [mF cm^{-2}]	Condition
Stretchability	MnO$_2$/CNT-coiled fiber (present work)	2.72	61.25	CV[a] at 10 mV s^{-1}
	CNT spring fiber[24]	0.51	27.07	GCD[b] GCD at 424 μA cm^{-2}
	Buckled MnO$_2$/CNT fiber[23]	0.26	27.98	CV at 10 mV s^{-1}
	All graphene core–sheath fiber[9]	0.02	1.7	CV at 50 mV s^{-1}
Flexibility	MnO$_2$/CNT fiber[2]	0.019	3.57	GCD at 0.5 μA
	MnO$_2$/ZnO nanowires/polymer fiber[16]	0.02	2.4	CV at 100 mV s^{-1}
	Graphene fiber[8]	0.01	0.72	GCD at 424 μA cm^{-2}
	TiO$_2$/CNT fiber[3]	0.024	0.6	GCD at 0.25 μA
	CNT fiber, CNT film[4]	0.029	8.66	GCD at 1 μA
	PEDOT/CNT fiber[1]	0.47	73	CV at 10 mV s^{-1}
	Graphene/CNT fiber[5]	0.027	4.97	GCD at 0.04 A g^{-1}
	ZnO nanowire/graphene fiber[10]	0.025	0.4	CV at 100 mV s^{-1}
	Pen ink/carbon, metal fiber[15]	1.008	26.4	CV at 100 mV s^{-1}

[a]Cyclic voltammograms (CV); [b]Galvanostatic charge–discharge test (GCD).

tensile strains from 20% to 40% with sequentially 5% increments to the hybrid coiled electrode (Figure 4B). It is notable that the coiled electrode can be stretched up to 40% and reversibly recovered without significant residual deformation (less than 2.5%). This stretchable electrode's mechanical reversibility has not been reported among other stretchable FBSs.[19–24] In addition, the constant slopes of the loading curves exhibit high modulus from 290 ($\varepsilon = 20\%$) to 325 MPa ($\varepsilon = 40\%$), while hysteretic energy dissipations by the recovery friction force were observed during unloading.[29] The capacitance retention of the coiled supercapacitor under mechanically static strain (2% s^{-1}) is characterized by comparing its CV curves before and after 37.5% strain was applied, as shown in Figure 4C. Figure 4D shows static capacitance retention with a strain range from 20% to 40% before the coiled yarn breaks. The coiled supercapacitor exhibits about 84% capacitance retention at the maximum strain of 37.5%. This capacitance drop can be attributed to a linear resistance increase of the coiled electrode when it gets stretched.[29] The inset shows SEM images of microloops before and after 37.5% stretching, showing reversible intercoil distance change.

Based on target applications of power source for wearable electronics, it is necessary to characterize the dynamic electrochemical performance[30] of stretchable supercapacitor by measuring real-time capacitance retention under dynamically applied strain. To guarantee reliable elasticity with negligible residual deformation, the following dynamic characterizations were performed with a moderate strain of 20%.[29] **Figure 5**A–C show dynamically measured CV curves of the coiled supercapacitor with various

strain rates. Applied strain rates of 2, 4, and 6% s^{-1} can be converted into frequencies of 0.1, 0.2, and 0.3 Hz for a stretching, respectively, which are close to that of human motion-based movements (0.67–4 Hz).[31] In the static mode, the coiled supercapacitor can retain 90% capacitance at 20% strain and reversibly recovered its initial capacitance when released (Figure S5, Supporting Information). Therefore, dynamic capacitance variation (capacitance decrease during yarn stretching and recovery during releasing) results in dynamic CV curves with an uneven contour during the tests (Figure 5A–C). Because it takes 10 s for the coiled supercapacitor to reach 20% strain at 2% s^{-1} strain rate (Figure 5A), a single stretching/releasing cycle is included per CV cycle measured at 100 mV s^{-1} scan rate. Similarly, two and three stretching/releasing cycles are included per CV cycle at 4 and 6% s^{-1} strain rates, respectively (Figure 5B,C). The resulting dynamic capacitance retentions at various strain rates are summarized in Figure 5D. Owing to highly adhesive MnO$_2$ shell formation on the yarn electrode, structural stability, and stable ion supply by the gel electrolyte of the coiled supercapacitor, it exhibits 95.5, 96.2, and 96.3% dynamic capacitance retention at 2, 4, and 6% s^{-1} strain rates without any electrical short circuit or significant performance degradation.

To characterize the reliability of electrochemical performances of the coiled supercapacitor, repeated stress loading/unloading and charge/discharge cycles were independently conducted. With a moderate strain of 20%, the coiled supercapacitor showed capacitance retentions of 95% after 1000 stretching/releasing cycles and 98.8% after 1000 charge/discharge cycles (Figure S6A, Supporting Information). Good adhesion between the MnO$_2$ shell and CNT core can be also confirmed through SEM images (Figure S6B, Supporting Information). After the cycle tests, the MnO$_2$ shell still remains in a well-attached state over the whole electrode without any observable detachment or cracks. On the other hand, the MnO$_2$ shell deposited onto the smooth surface carbon fiber shows significant detachment after the cycle tests, implying poor adhesion to the electrode (Figure S7, Supporting Information). This is because the unique surface and internal porosities of twist spun-based CNT yarn[32] have advantages to have good adhesion with active material. Therefore, this simple way for nanoscopic MnO$_2$ deposition effectively provides strong adhesion to the surface of the bare coiled electrode as well as enhancing the energy storage performance without impairing mechanical stretchability or electrochemical cyclability.

In summary, we have reported stretchable and highly performing yarn-based supercapacitors that use unique core–shell-structured coiled electrodes. Pseudocapacitive core(CNT)–shell(MnO$_2$)-structured yarns were prepared using an electrochemical method and the resulting solid-state coiled supercapacitor exhibits high elasticity, specific capacitances, and mechanical, electrochemical cyclabilities. The linear and volumetric capacitances of the coiled supercapacitor were 2.72 mF cm^{-1} and 34.6 F cm^{-3}, respectively. About 84% static capacitance was retained when it was reversibly stretched by 37.5% in strain while 96.3% dynamic capacitance was retained during 20% strain deformation despite the extremely high strain rate of 6% s^{-1}. Owing to the active material's strong adhesion and structural stability of the coiled electrode, the coiled supercapacitor exhibited 95% and 98.8% capacitance retentions
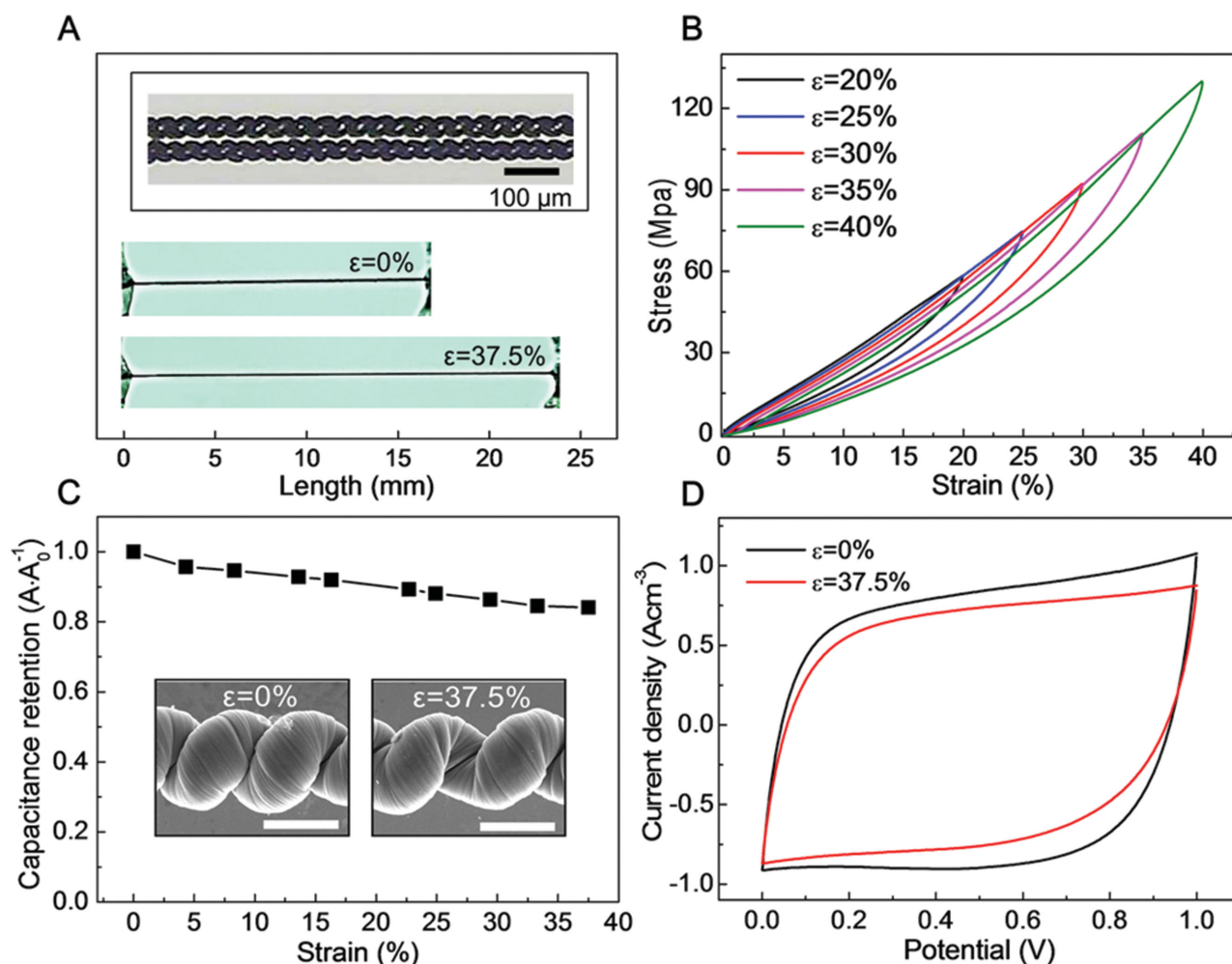
Figure 4. A) Optical images of solid-state coiled supercapacitor before and after application of 37.5% tensile strain. The initial length of as-used coiled supercapacitor is 16.8 mm for the stretching test. Inset shows magnified coiled supercapacitor, which was assembled using two parallel coiled electrodes with a constant gap (≈20 μm gap, scale bar = 100 μm). B) Stress loading/unloading curves of the hybrid MnO$_2$/CNT coiled electrode with tensile strains from 20% to 40%. C) Static CV curve comparison before (black line) and after 37.5% strain applied (red line) to the coiled supercapacitor, showing 84% capacitance retention. D) Capacitance retention versus static strain. The inset shows magnified SEM images of microloops before and after 37.5% strain applied (scale bar = 50 μm).

after stretching/releasing and charge/discharge cycles, respectively. Because we have deployed the twist insertion-based coiling method to obtain a highly elastomeric electrode, the presently described supercapacitor fabrication method can be extended to other diverse high-strength monofilament and multifilament polymer fibers (such as polyethylene, Kevlar, silver-plated nylon, polyester, polypropylene, and poly(vinylidene difluoride)) to make supercapacitors that operate at high temperatures and use either hydrophilic or hydrophobic electrolytes.

Experimental Section

CNT forests (≈400 μm high and consisting of ≈12 nm diameter nanotubes containing ≈9 walls) were synthesized using the chemical vapor deposition (CVD) method according to a previous report.[25] Ten layers of 120 mm (length) × 10 mm (width) sized CNT sheets were drawn from the forest and stacked on the glass substrate by ethanol evaporation-based densification. One end of the stacked sheet was

connected to the electrical motor for coil twisting. The bare CNT coiled yarn electrodes were fabricated by inserting a giant twist (≈50,000 twisting per meter) into CNT sheets. The prepared coiled yarn was electrically connected to 180 μm diameter Cu wire using silver paste for MnO$_2$ deposition and electrochemical performance characterization. The electrochemical MnO$_2$ deposition on the pristine CNT coiled yarn was performed using a potentiostatic method of applying 1.3 V (vs Ag/AgCl as reference electrode and Pt mesh as counter electrode) in the three electrode of CHI 627b system (CH Instruments, Austin, TX) in an electrolyte containing 0.02 M MnSO$_4$·5H$_2$O and 0.2 M Na$_2$SO$_4$ (all chemical products were purchased from Sigma Aldrich). Deposition time for one deposition segment was 3 s and the number of segments was controlled to adjust the deposition amount. The mass of the MnO$_2$ was measured using EQCM and calculated using the Sauerbrey equation.[33] The PVA–LiCl gel electrolyte was prepared using 3 g PVA (M_w 146,000–186,000) and 6 g LiCl in 30 mL deionized water. The mixture was heated at 90 °C until it became transparent. Two symmetric MnO$_2$/CNT core–shell-structured coiled electrodes were placed in a parallel direction with a small gap (≈20 μm) and finally coated with the PVA–LiCl gel electrolyte to complete the fabrication of the coiled supercapacitor. All chemical reagents for solid-electrolyte synthesis were purchased from Sigma

www.MaterialsViews.com

ADVANCED
ENERGY
MATERIALS
www.advenergymat.de

COMMUNICATION
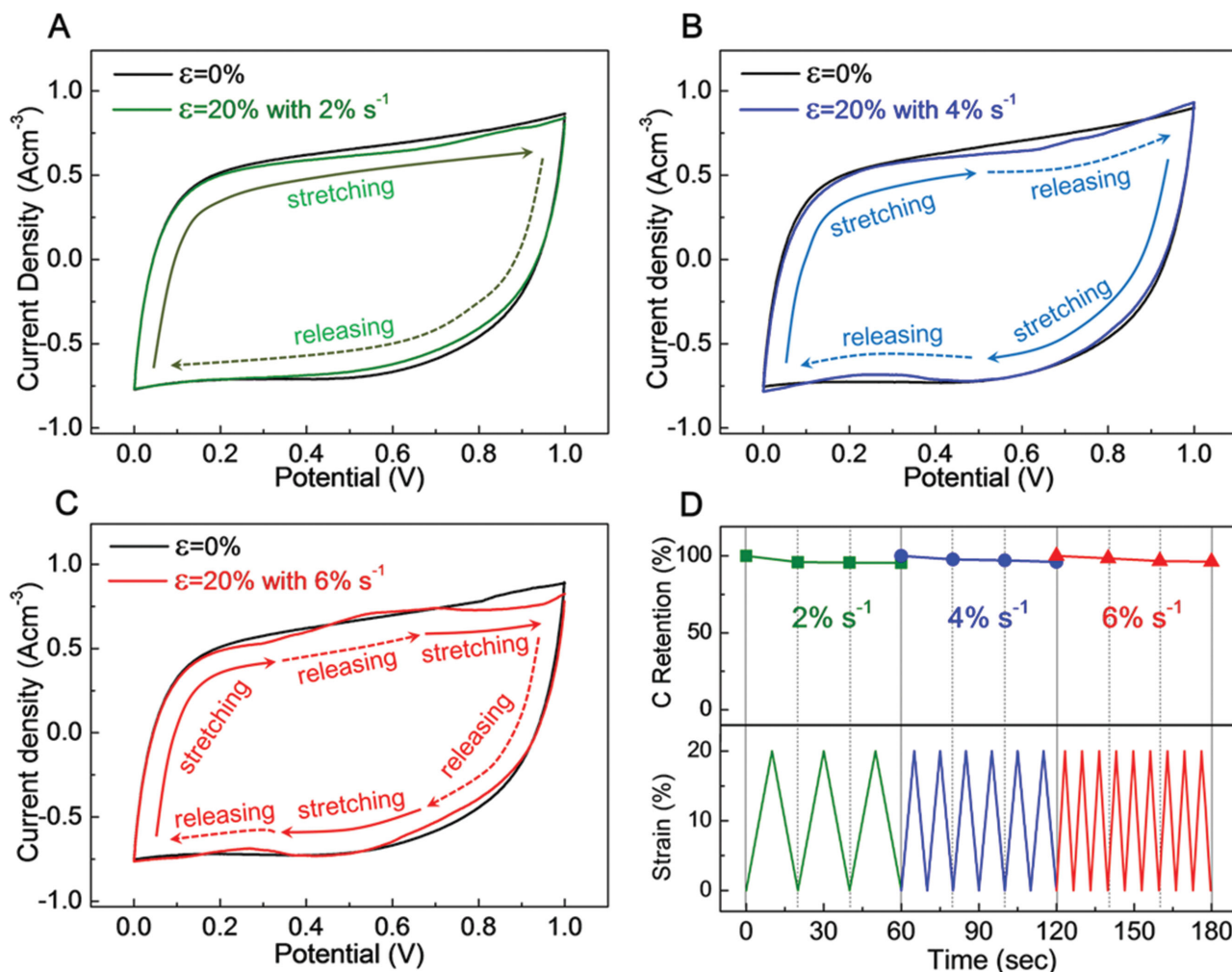
Figure 5. Dynamically measured CV curves (at 100 mV s^{-1} scan rate) during 20% strain stretching/releasing cycles with various strain rates. Non-stretched ($\varepsilon = 0$) coiled supercapacitor's CV curves are denoted for comparison (black line), while the dynamically measured CV curves with strain rates of A) 2% s^{-1} (green line, 10 s for full stretching), B) 4% s^{-1} (blue line, 5 s for full stretching), and C) 6% s^{-1} (red line, 3.3 s for full stretching) are presented. D) Overall dynamic capacitance retentions of a coiled supercapacitor, showing 95.5%, 96.2%, and 96.3% retentions at 2, 4, and 6% s^{-1} strain rates, respectively, after three charge/discharge cycles.

Aldrich and used without further processing. To characterize the hybrid core–shell structure of the coiled electrode, cross-sections of the coil were prepared by cutting them along their diameters using a Ga ion beam (7 nA beam current) in a Focused Ion Beam (FIB, Nova 200) operated at 30 kV. Then, the cut areas were cleaned via Ga ion polishing by etching several micrometers of yarn length with consecutively decreasing ion beam-currents ranging from 5.0 to 0.3 nA. The clean-cut yarns were next transferred to a Zeiss Supra 40 SEM to perform the microscopy (at 15 kV) and elemental EDAX mapping analysis (at 20 kV). Clear views of the yarn's cross-sections were attained by orienting the yarn's cut plane parallel to the electron-beam final aperture/detector in the SEM. Other SEM images were obtained by FE-SEM (S4700, Hitachi). The oxidation state of the MnO$_2$ deposit was characterized by XPS analysis (VG Multilab ESCA 2000 system). All static electrochemical measurements on the coiled supercapacitor utilized a two-electrode configuration with electrochemical analyzer (CHI 627b, CH Instruments). Dynamic CV curves were measured (100 mV s^{-1}) while the coiled supercapacitor was stretched and released at strain rates of 2, 4, and 6% s^{-1} (which can be converted into 180–540 mm min^{-1}). A specially constructed machine for applying tensile deformations was used. The length of the supercapacitor was measured using a digital Vernier caliper (500 series, Mitutoyo), which was incorporated into the stretching machine. Stress

loading–unloading curves were obtained using a mechanical analyzer (TMA, SS7100). The volumetric capacitance of the coiled supercapacitor was calculated from the CV curves. From $C = I/(dV/dt)$, where I is the discharge current, the single-electrode specific capacitance (C_{sp}) was calculated from the following equation.[1]

$$C_{sp}(F/cm^3) = \frac{4C}{Vol_{electrode}}, \qquad (1)$$

where $Vol_{electrode}$ is the total volume of the electrochemical active materials of the two electrodes (MnO$_2$/CNT coiled electrodes for the present work). In a similar way, total length and surface area of the active materials were used for linear and areal capacitance calculations, respectively. The factor of 4 comes from the capacitance of the two-electrode system and the combined volume of the two electrodes.[1]

Supporting Information

Supporting Information is available from the Wiley Online Library or from the author.

COMMUNICATION

[1] J. A. Lee, M. K. Shin, S. H. Kim, H. U. Cho, G. M. Spinks, G. G. Wallace, M. D. Lima, X. Lepro, M. E. Kozlov, R. H. Baughman, S. J. Kim, *Nat. Commun.* **2013**, *4*, 1970.

[2] J. Ren, L. Li, C. Chen, X. Chen, Z. Cai, L. Qiu, Y. Wang, X. Zhu, H. Peng, *Adv. Mater.* **2013**, *25*, 1155.

[3] T. Chen, L. Qiu, Z. Yang, Z. Cai, J. Ren, H. Li, H. Lin, X. Sun, H. Peng, *Angew. Chem. Int. Ed.* **2012**, *51*, 11977.

[4] X. Chen, L. Qiu, J. Ren, G. Guan, H. Lin, Z. Zhang, P. Chen, Y. Wang, H. Peng, *Adv. Mater.* **2013**, *25*, 6436.

[5] H. Sun, X. You, J. Deng, X. Chen, Z. Yang, J. Ren, H. Peng, *Adv. Mater.* **2014**, *26*, 2868.

[6] B. Wang, X. Fang, H. Sun, S. He, J. Ren, Y. Zhang, H. Peng, *Adv. Mater.* DOI: 10.1002/adma.201503441.

[7] G. Sun, X. Zhang, R. Lin, J. Yang, H. Zhang, P. Chen, *Angew. Chem.* **2015**, *127*, 4734.

[8] Q. Chen, Y. Meng, C. Hu, Y. Zhao, H. Shao, N. Chen, L. Qu, *J. Power Sources* **2014**, *247*, 32.

[9] Y. Meng, Y. Zhao, C. Hu, H. Cheng, Y. Hu, Z. Zhang, G. Shi, L. Qu, *Adv. Mater.* **2013**, *25*, 2326.

[10] J. Bae, Y. J. Park, M. Lee, S. N. Cha, Y. J. Choi, C. S. Lee, J. M. Kim, Z. L. Wang, *Adv. Mater.* **2011**, *23*, 3446.

[11] Y. Ma, P. Li, J. W. Sedloff, X. Zhang, H. Zhang, J. Liu, *ACS Nano* **2015**, *9*, 1352.

[12] Y. Liang, Z. Wang, J. Huang, H. Cheng, F. Zhao, Y. Hu, L. Jiange, L. Qu, *J. Mater. Chem. A* **2015**, *3*, 2547.

[13] X. Xiao, T. Li, P. Yang, Y. Gao, H. Jin, W. Ni, W. Zhan, X. Zhang, Y. Cao, J. Zhong, L. Gong, W. C. Yen, W. Mai, J. Chen, K. Huo, Y. L. Chueh, Z. L. Wang, J. Zhou, *ACS Nano* **2012**, *6*, 9200.

[14] D. Yu, S. Zhai, W. Jiang, K. Goh, L. Wei, X. Chen, R. Jiang, Y. Chen, *Adv. Mater.* **2015**, *27*, 4895.

[15] Y. Fu, X. Cai, H. Wu, Z. Lv, S. Hou, M. Peng, X. Yu, D. Zou, *Adv. Mater.* **2012**, *24*, 5716.

[16] J. Bae, M. K. Song, Y. J. Park, J. M. Kim, M. Liu, Z. L. Wang, *Angew. Chem. Int. Ed.* **2011**, *50*, 1683.

[17] M. D. Lima, N. Li, M. J. Andrade, S. Fang, J. Oh, G. M. Spinks, M. E. Kozlov, C. S. Haines, D. Suh, J. Foroughi, S. J. Kim, Y. Chen, T. Ware, M. K. Shin, L. D. Machado, A. F. Fonseca, J. D. W. Madden, W. E. Voit, D. S. Galvao, R. H. Baughman, *Science* **2012**, *338*, 928.

[18] C. Yan, J. Wang, W. Kang, M. Cui, X. Wang, C. Y. Foo, K. J. Chee, P. S. Lee, *Adv. Mater.* **2013**, *26*, 2022.

[19] Z. Zhang, J. Deng, X. Li, Z. Yang, S. He, X. Chen, G. Guan, J. Ren, H. Peng, *Adv. Mater.* **2014**, *27*, 356.

[20] Y. Zhang, W. Bai, X. Cheng, J. Ren, W. Weng, P. Chen, X. Fang, Z. Zhang, H. Peng, *Angew. Chem. Int. Ed.* **2014**, *53*, 14564.

[21] C. Choi, S. H. Kim, H. J. Sim, J. A. Lee, A. Y. Choi, Y. T. Kim, X. Lepro, G. M. Spinks, R. H. Baughman, S. J. Kim, *Sci. Rep.* **2015**, *5*, 9387.

[22] P. Xu, T. Gu, Z. Cao, B. Wei, J. Yu, F. Li, J. H. Byun, W. Lu, Q. Li, T. W. Chou, *Adv. Energy Mater.* **2014**, *4*, 1300759.

[23] P. Xu, B. Wei, Z. Cao, J. Zheng, K. Gong, F. Li, J. Yu, Q. Li, W. Lu, J. H. Byun, B. S. Kim, Y. Yan, T. W. Chou, *ACS Nano* **2015**, *9*, 6088.

[24] T. Chen, R. Hao, H. Peng, L. Dai, *Angew. Chem. Int. Ed.* **2015**, *54*, 618.

[25] M. Zhang, K. R. Atkinson, R. H. Baughman, *Science* **2004**, *306*, 1358.

[26] G. Yu, L. Hu, M. Vosgueritchian, H. Wang, X. Xie, J. R. McDonough, X. Cui, Y. Cui, Z. Bao, *Nano Lett.* **2011**, *11*, 2905.

[27] X. Dong, X. Wang, J. Wang, H. Song, X. Li, L. Wang, M. B. Chan-Park, C. M. Li, P. Chen, *Carbon* **2012**, *50*, 4865.

[28] S. W. Lee, J. Kim, S. Chen, P. T. Hammond, Y. Shao-Horn, *ACS Nano* **2010**, *4*, 3889.

[29] Y. Shang, X. He, Y. Li, L. Zhang, Z. Li, C. Ji, E. Shi, P. Li, K. Zhu, Q. Peng, C. Wang, X. Zhang, R. Wang, J. Wei, K. Wang, H. Zhu, D. Wu, A. Cao, *Adv. Mater.* **2012**, *24*, 2896.

[30] X. Li, T. Gu, B. Wei, *Nano Lett.* **2012**, *12*, 6366.

[31] S. Jung, J. Lee, T. Hyeon, M. Lee, D. H. Kim, *Adv. Mater.* **2014**, *26*, 6329.

[32] C. Choi, J. A. Lee, A. Y. Choi, Y. T. Kim, X. Lepro, M. D. Lima, R. H. Baughman, S. J. Kim, *Adv. Mater.* **2014**, *26*, 2059.

[33] S. L. Kuo, N. L. Wu, *J. Electrochem. Soc.* **2006**, *153*, A1317.